Chlorination Chemistry. 2. Rate Coefficients, Reaction Mechanism, and Spectrum of the Chlorine Adduct of Allene

Dean B. Atkinson*,† and Jeffrey W. Hudgens*

Physical and Chemical Properties Division, Chemical Science and Technology Laboratory, National Institute of Standards and Technology, Gaithersburg, Maryland 20899

Received: August 2, 1999; In Final Form: November 24, 1999

Cavity ring-down (CRD) spectroscopy and ab initio calculations have determined the reaction rate coefficients, mechanism, and thermochemistry relevant to the addition of a chlorine atom to allene. Chlorine atoms were produced by laser photolysis at 351 nm and the addition reaction products were probed at a variable delay by CRD spectroscopy using a second laser pulse. Ab initio results indicate that the only persistent addition product is the 2-chloroallyl (C_3H_4Cl) radical. We measured the continuum spectrum of the 2-chloroallyl radical between 238 and 252 nm and determined the absorption cross section, $\sigma_{240}(C_3H_4Cl) = (2.5 \pm 0.5) \times 10^{-17}$ cm^2. By fitting the C_3H_4Cl absorption data to complex kinetic mechanisms, rate coefficients at 298 K were found to be $k(Cl+C_3H_4$; 656 Pa, $N_2) = (1.61 \pm 0.27) \times 10^{-10}$ cm^3 molecule^{-1} s^{-1}, $k(Cl+C_3H_4$; 670 Pa, He) $= (1.34 \pm 0.24) \times 10^{-10}$ cm^3 molecule^{-1} s^{-1}, and $k(Cl+C_3H_4$; 1330 Pa, He) $= (1.75 \pm 0.25) \times 10^{-10}$ cm^3 molecule^{-1} s^{-1}. The rate coefficient of the self-reaction displayed no pressure dependence between 434 and 1347 Pa in N_2 buffer giving $k(C_3H_4Cl+C_3H_4Cl) = (3.7 \pm 1.0) \times 10^{-11}$ cm^3 molecule^{-1} s^{-1}. A study of the addition reaction of 2-chloroallyl radical and oxygen molecule determined σ_{240} $(C_3H_4ClO_2) = (3.6 \pm 0.7) \times 10^{-18}$ cm^2 and $k(O_2+C_3H_4Cl$, 705 Pa $N_2) = (3.6 \pm 0.4) \times 10^{-13}$ cm^3 molecule^{-1} s^{-1}. The listed uncertainties denote two standard deviations, and those for rate coefficients include the uncertainty of the appropriate absorption cross section.

Introduction

During the incineration process, pyrolysis of organic waste can produce allene (CH_2═C═CH_2) that may subsequently react with the chlorine atoms liberated by oxidation of chlorinated species.[1] Under conditions characterized by incomplete mixing, the initial chlorinated organic product may feed into reaction sequences that produce an undesirable, highly chlorinated, inert effluent. Despite its important role during incineration, the reaction of chlorine and allene is little studied. The available data indicate that the reaction is very rapid. Wallington et al.[2] measured the total reaction rate coefficient, $k(Cl+C_3H_4) = (4.38 \pm 0.26) \times 10^{-10}$ cm^3 molecule^{-1} s^{-1} at 298 K and atmospheric pressure. More recently, Farrell and Taatjes [3] used diode laser spectroscopy to probe the HCl product of this reaction over a broad temperature range. They observed $k(Cl+C_3H_4) = (2.49 \pm 0.52) \times 10^{-10}$ cm^3 molecule^{-1} s^{-1} at 298 K and in 1333 Pa (10 Torr) CO_2 buffer. Their kinetic data showed evidence for two reaction channels:

$$H_2C{=}C{=}CH_2 + Cl\ (+M) \rightarrow HCl + C_3H_3 \qquad (1a)$$

$$\rightarrow C_3H_4Cl \qquad (1b)$$

where C_3H_3 was assumed to be the propargyl ($^{\bullet}CH_2C{\equiv}CH$) radical and C_3H_4Cl was assigned to be the 2-chloroallyl (CH_2-$CClCH_2$) radical. Farrell and Taatjes[3] found that the branching ratio of product channels 1a and 1b changed as a function of temperature. At 298 K, they observed little HCl product and concluded that hydrogen abstraction accounted for ∼2% of the reactivity. This result indicates that chlorine addition (reaction 1b) dominates the total reactivity. At higher temperatures, the HCl product fraction increased and became unity near 800 K. In accord with these 298 K results, we recently reported that the reaction of Cl + allene does not produce detectable concentrations of propargyl (C_3H_3) radicals.[4] The dominance of the chlorine addition channel in allene near 298 K is consistent with the reactive behavior of most unsaturated hydrocarbons.

The radical isomer formed by reaction 1b is not fully established. By using a partial energy diagram of the reaction intermediates, Farrell and Taatjes[3] accounted for the branching ratio between HCl and adduct formation for reaction 1. From this analysis, they suggested that the 2-chloroallyl radical is the dominant addition product. These computational results did not address the production of a persistent 3-chloro-1-propene-2-yl radical population, nor did the computations rule out production of the 1-chloroallyl radical, which is the most stable product available to reaction 1b.

The expectation that reaction 1b yields exclusively 2-chloroallyl radicals is presaged by early studies of the bromine atom reaction with allene.[5,6] Researchers have photolyzed HBr/allene mixtures under conditions that minimized heterogeneous reactions and analyzed the stable end products. These analyses found that all newly added halogen atoms resided on the center carbon, suggesting that the persistent gas-phase adduct radical is the 2-bromoallyl radical. Because the energy surfaces governing bromine and chlorine addition to allene are expected to be similar, we may also expect reaction 1b to produce 2-chloroallyl radicals exclusively. Interestingly, end product analyses say little conclusive about the reaction mechanism. The 2-haloallyl radical

* Corresponding author. E-mail: jeffrey.hudgens@nist.gov. E-mail: atkinsond@pdx.edu.

† NIST/NRC Postdoctoral Associate 1995−97. Current address: Chemistry Department, Portland State University, Portland, OR 97207-0751.

10.1021/jp9927247 CCC: $19.00
Published on Web 01/12/2000

may form directly by halogen addition onto the center carbon, or it may form via a mechanism involving halogen addition onto an end carbon followed by a transfer of the halogen to the center carbon. In a subsequent report, we will resolve these mechanistic details using the results of high-level ab initio calculations.[7]

In this report, we describe the ultraviolet absorption (UV) spectrum between 238 and 252 nm of C_3H_4Cl radicals produced by reaction 1b. We observed this spectrum using an apparatus that integrates in situ laser photolytic production of radicals with a cavity ring-down (CRD) spectroscopic detector. Using a chemical actinometric procedure, we have determined the absorption cross sections of the 2-chloroallyl radical at 240 nm. We report kinetics experiments that measured the rate coefficients at 298 K for the chlorine atom addition to allene (reaction 1b), the self-reaction of C_3H_4Cl, and the reaction of C_3H_4Cl with O_2. We present ab initio computational results that strongly support the conclusion that the reactive species is the 2-chloroallyl radical. The ab initio calculations also allow us to speculate upon the electronic transition that produces the absorption signal.

Experimental Procedure[8]

The details of the laser photolysis/cavity ring-down (CRD) apparatus are comprehensively described elsewhere,[9] so this section presents only a basic overview and recent refinements. A 16 mm ID quartz tube forms the reactor through which a flowing mixture of known composition is passed. The pumping rate is adjusted so that the movement of the gas sample along the flow axis is inconsequential within the time interval of a single kinetic measurement, yet fast enough that the reaction mixture is fully refreshed during the 200 ms between laser pulses. Chlorine (10.5% Cl_2 of 99.7% purity) in He (99.995% purity) and allene (97% containing 1.0% propyne as determined by gas chromatography) were used as supplied and flowed through mass flow controllers.

Initially, a XeF excimer laser (351 nm, nominal 20 ns pulse, max pulse energy 200 mJ) photolyzes the reaction mixture. The photolysis laser beam is expanded and masked to produce a uniform block 67 mm wide and 20 mm high with a peak power density of less than 100 kW/cm^2. Subsequently, the absorption by a selected species is measured with cavity ring-down absorption spectroscopy. For the cavity ring-down spectroscopy measurements, we used a 1.1 m long cavity formed by two 1.0 m radius of curvature mirrors of high peak effective reflectivity ($R^* > 99.6\%$ @ 245 nm) and a usable bandwidth of about ± 7 nm ($R^* > 98\%$.) At 245 nm, the cavity exhibited an exponential decay with a base 1/*e* ring down time of 1.3 μs. The ring-down cavity lies along the flow axis, normal to the photolysis beam direction, so that the width of the photolysis beam defines the path length of the transient absorbing species. This optical configuration makes the extraction of species density straightforward. To minimize effects from radial gradients of photolysis products, the photolysis beam height is larger than the diameter of the reactor tube and the probe beam diameter inside the cavity (beam waist of $TEM_{max} \approx 0.32$ mm) is much smaller than the flow tube inner dimension.

The tunable probe laser beam was produced by an excimer pumped dye laser (nominal 20 ns pulse width; laser dye: coumarin 480; BBO doubling crystal). At the cavity entrance mirror, the probe beam passed through a 2 mm diameter iris and the pulse energy was not allowed to exceed 100 μJ/cm^2. The photomultiplier signal was (analog) filtered to pass frequencies less than 25 MHz. (Proper cavity alignment was verified by observing oscilloscope traces recorded at the full 1.0 GHz bandwidth.) A weighted fit to each exponential ring-down trace was extracted from a linear regression of a semilog plot and yielded the decay rate.

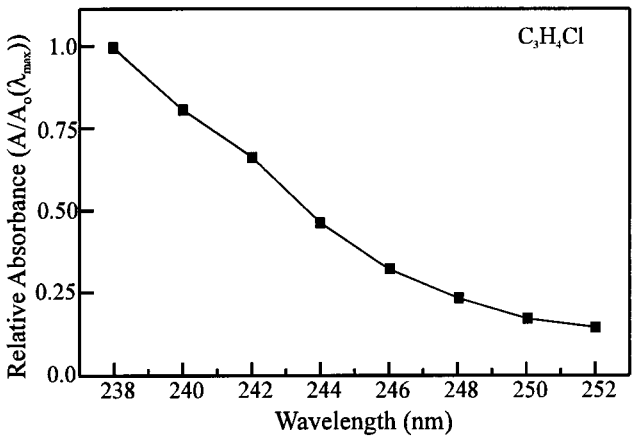

Figure 1. Ultraviolet absorption spectrum between 238 and 252 nm of the 2-chloroallyl (C_3H_4Cl) radical produced by reaction 1.

Cavity ring-down measurements observe the enhanced rate of decay of photon intensity in a stable optical cavity and readily convert this into absorbance when the decay rate under nonabsorbing conditions (base decay rate) is known. In this experiment, the base decay rate is measured by probing the reaction mixture prior to the photolysis laser pulse. The decay or growth of the monitored species absorption is observed by changing the delay time between the photolysis and probe (CRD) laser pulses. To minimize the effects of long-term drift in the photolysis efficiency, the time interval between the pulses is randomly selected between zero and preset values.

The kinetics experiments observe data comprised of transient absorbance vs time. We used absorption cross sections to convert this absorbance into radical concentrations. To derive rate coefficients from these data, we designed a kinetic mechanism composed of the active chemical reaction steps and simulated the absorption data on a computer using the ACUCHEM kinetics simulation program.[10] This simulated absorption profile was compared to the observed data, and the χ^2 value was computed. Using the Levenberg−Marquardt procedure, selected rate coefficients and concentrations are varied to minimize the χ^2 value, thus determining the unknown rate coefficients.[11]

Ab initio calculations were performed with the Gaussian 94 program suite.[12]

Experimental Results

Transient CRD Spectrum. When exposed to 351 nm light, mixtures containing chlorine, allene, and N_2 displayed transient absorption signals between 238 and 252 nm manifesting fast 1/*e* rise times ($t_{rise} \approx 10-80$ μs) and slower 1/*e* fall times ($t_{fall} \approx 1-7$ ms). Respectively, the rise and fall rates have first-order and second-order decay signatures. Mixtures absent of Cl_2 produced no transient signal. These results are consistent with the reaction sequence:

$$Cl_2 + 351\ nm \rightarrow 2Cl \qquad (2)$$

$$H_2C{=}C{=}CH_2 + Cl\ (+M) \rightarrow C_3H_4Cl \qquad (1b)$$

$$C_3H_4Cl + C_3H_4Cl\ (+M) \rightarrow products \qquad (3)$$

Figure 1 shows a transient low-resolution absorption spectrum obtained 200 μs after the photolysis event. The onset of

significant absorption lies at 252 nm, and absorption strength increases at shorter wavelength. Since the absorption strength is still increasing at the blue wavelength limit of our CRD mirrors, the true absorption maximum of this electronic transition probably resides at a shorter wavelength than 238 nm.

By exposing allene and propyne to 193 nm light, we produced propargyl (C_3H_3) radicals[4,13] and examined the spectral intervals between 310 and 360 nm and between 238 and 252 nm. Between 310 and 360 nm, we observed the well-known $\tilde{A}-\tilde{X}^2B_1$ bands of propargyl radicals.[4,13,14] Between 238 and 252 nm, we detected no transient absorption, establishing that propargyl radicals do not absorb over this spectral interval. Thus, the accumulated data establish that the absorption spectrum (Figure 1) arises only from C_3H_4Cl radicals produced by reaction 1b. In the Discussion section of this paper, we use the results of ab initio calculations to establish that reaction 1b produces only one C_3H_4Cl isomer radical, the 2-chloroallyl radical. In this view, the optical absorption cross section and kinetic rate coefficients reported below are fundamental properties of the 2-chloroallyl radical.

Optical Absorption Cross Section Measurements. The absorption cross section of the 2-chloroallyl (C_3H_4Cl) radical was determined at 240 nm using chemical actinometry. Within the bandwidth of our laser ($\Delta\nu \approx 0.3$ cm^{-1}), the spectrum exhibits no evidence of fine structure, indicating that this band is an absorption continuum at 240 nm. Such diffuse continuum spectra are ideal for absorption measurements with cavity ring-down spectroscopy. The extinction coefficient remains essentially constant across the bandwidth of the laser beam causing each populated cavity mode to decay at the same rate.[15] The uniformity of these decay rates enables accurate concentration measurements.

We established the absolute absorption cross section of the C_3H_4Cl radical at 240 nm by comparing it with the absorption cross section of ethylperoxy ($C_2H_5O_2$) radical. For these experiments, a mixture of helium buffer and 10% chlorine in He with a large stoichiometric excess of allene was flowed through the reactor. The photolysis pulse from a XeF laser produced Cl atoms which rapidly reacted with allene (reactions 2 and 1). The maximum transient absorbance from C_3H_4Cl radicals was measured by CRD spectroscopy at 240 nm. Immediately following this measurement, the allene flow was replaced by ethane and O_2 and the absorption experiment was repeated. The excimer laser generated chlorine atoms that reacted through the sequence

$$Cl + C_2H_6 \rightarrow HCl + C_2H_5 \quad (4)$$

$$C_2H_5 + O_2\ (+M) \rightarrow C_2H_5O_2 \quad (5)$$

Sufficient ethane and oxygen were added to ensure that >98% of the chlorine atoms produced in reaction 2 were converted to ethylperoxy radicals.[9,16] Since the chlorine flow rate and excimer laser energy remained constant throughout these steps, the initial concentration of photolytic chlorine atoms, $[Cl]_0$, is presumed to be identical for both measurements. Thus, the CRD absorption measurements assayed equal amounts of C_3H_4Cl and $C_2H_5O_2$ radicals. The ratio of absorbances, $A_{240}^{C_3H_4Cl}/A_{240}^{C_2H_5O_2} = 5.80 \pm 0.07$, was multiplied by the recommended absorption cross section of ethylperoxy radical at 240 nm, $\sigma_{240}(C_2H_5O_2) = (436 \pm 80) \times 10^{-20}$ cm^2,[16,17] to yield a value of $\sigma_{240}(C_3H_4Cl) = (2.5 \pm 0.5) \times 10^{-17}$ cm^2 for the C_3H_4Cl radical absorption cross section, where the stated uncertainty is twice the standard deviation of the determination.

Determination of the Rate Coefficients, k_1(Cl + C_3H_4) and k_3(C_3H_4Cl + C_3H_4Cl). The formation rate coefficient (reaction 1b) and the self-reaction rate coefficient (reaction 3) of C_3H_4Cl radicals were studied at 298 K by observing the change of absorbance at $\lambda_{crd} = 240$ nm following the 351 nm photolysis of Cl_2 in 33 separate experiments. Table 1 lists the chemical conditions, derived rate coefficient, and fit precision obtained for each experiment. Figure 2 shows two such experiments that monitored optical absorbance by C_3H_4Cl at 240 nm as a function of time.

During each kinetic experiment, we measured the average photolysis energy transmitted through the flow reactor and found that it diminished by less than 1%. The average photolysis flux across the entire sample is uniform within 10%. This uniformity characteristic exists because the photolysis beam impinges perpendicular to the CRD cavity, the probe beam diameter inside the cavity is small, and the gas mixture is optically thin. We also experimentally verified that each photolysis event irradiated only fresh gas samples. When allene is photolyzed with 193 nm light, a weak absorption appears promptly at $\lambda_{crd} = 240$ nm that exhibits no transient decay. This small absorbance does not cease until the irradiated sample has exited the flow reactor. Although we could not identify the carrier (and its appearance is too prompt to attribute to soot formation), this signal was used to establish the gas flow conditions that assured that each experiment involved a fresh gas sample. Since allene is transparent to 351 nm light, this offset absorbance did not appear during the kinetic measurements presented in this report. A numerical model of diffusion between the CRD axis and the reactor walls predicts that data observed at reaction times earlier than 20 ms will be unaffected by wall reactions. Since this study uses data observed at reaction times of 10 ms and less, we did not incorporate a wall reaction rate coefficient into our kinetic models.

Rate coefficients, $k_1(Cl + C_3H_4)$, were derived by measuring signal traces of 50−100 μs duration after the photolysis event and fitting these traces with a kinetic model composed of reactions 1, 2, and 3, where the fit coefficients of the model are also the rate coefficients. We fixed the self-reaction rate coefficient, $k_3(C_3H_4Cl + C_3H_4Cl)$, to the average values, given below. Figure 2a shows the data (squares) obtained by a typical experiment and the fit (solid line) that extracts k_1. The lower panel shows the residuals computed from the differences between the observed signal trace and the trace obtained by fitting the model. Fits of the present data display a dependence upon pressure and collision partner (Table 1), showing that our measurements were conducted within the reaction pressure falloff region of reaction 1. We report three distinct rate coefficients: $k_1(656\ Pa, N_2) = (1.61 \pm 0.27) \times 10^{-10}$ cm^3 molecule^{-1} s^{-1}, $k_1(670\ Pa, He) = (1.34 \pm 0.24) \times 10^{-10}$ cm^3 molecule^{-1} s^{-1}, and $k_1(1330\ Pa, He) = (1.75 \pm 0.25) \times 10^{-10}$ cm^3 molecule^{-1} s^{-1}, where the uncertainty denotes two standard deviations. Although this uncertainty includes the uncertainty of $\sigma_{240}(C_3H_4Cl)$, its contribution is negligible because the experiments are conducted under pseudo-first-order conditions.

Figure 2b shows a typical experimental trace (squares) and the fit (solid line) that extracts one measurement of the self-reaction rate coefficient, $k_3(C_3H_4Cl+C_3H_4Cl)$. The lower panel shows the residuals between the data and the best fit. Similar signal traces of 5 and 10 ms duration were recorded in predominantly N_2 buffer at total pressures ranging between 434 Pa (3.25 Torr) and 1347 Pa (10.1 Torr). Since the individual reaction rate coefficient determinations show no pressure dependence (Table 2), we report their average, $k_3(C_3H_4Cl+C_3H_4Cl) = (3.7 \pm 1.0) \times 10^{-11}$ cm^3 molecule^{-1} s^{-1}, where the stated uncertainty is two standard deviations and propagates the

TABLE 1: Experimental Conditions Used to Determine the Rate Coefficients Involving the 2-Chloroallyl Radical

total press (Pa)	partial press N_2 (Pa)	partial press He (Pa)	partial press C_3H_4 (Pa)	partial press Cl_2 (Pa)	partial press O_2 (Pa)	derived $k_1(Cl+C_3H_4Cl)$[a] cm^3 $molecule^{-1}$ s^{-1}	derived $k_3(C_3H_4Cl+C_3H_4Cl)$[a] cm^3 $molecule^{-1}$ s^{-1}	derived $k_7(O_2+C_3H_4Cl)$[a] cm^3 $molecule^{-1}$ s^{-1}
656.9	536.6	97.2	11.6	11.4		$(1.48 \pm 0.05) \times 10^{-10}$		
656.2	538.0	97.5	9.3	11.4		$(1.55 \pm 0.09) \times 10^{-10}$		
656.1	539.8	97.8	7.0	11.5		$(1.48 \pm 0.06) \times 10^{-10}$		
656.1	540.7	98.0	5.9	11.5		$(1.50 \pm 0.05) \times 10^{-10}$		
655.8	542.5	98.3	3.5	11.5		$(1.76 \pm 0.04) \times 10^{-10}$		
655.9	541.6	98.1	4.7	11.5		$(1.76 \pm 1.06) \times 10^{-10}$		
655.7	543.3	98.4	2.4	11.5		$(1.74 \pm 0.07) \times 10^{-10}$		
						k_1^{ave} (656 Pa, N_2) = $(1.61 \pm 0.27) \times 10^{-10}$		
1331.2		1320.8	3.1	7.3		$(1.76 \pm 0.09) \times 10^{-10}$		
1325.6		1316.6	1.6	7.4		$(1.74 \pm 0.08) \times 10^{-10}$		
						k_1^{ave} (1330 Pa, He)[b] = $(1.75 \pm 0.25) \times 10^{-10}$		
670.8		645.9	11.4	13.5		$(1.42 \pm 0.11) \times 10^{-10}$		
670.8		645.9	11.4	13.5		$(1.13 \pm 0.04) \times 10^{-10}$		
669.5		650.0	5.8	13.6		$(1.38 \pm 0.06) \times 10^{-10}$		
669.5		650.0	5.8	13.6		$(1.18 \pm 0.04) \times 10^{-10}$		
670.8		654.2	2.9	13.7		$(1.42 \pm 0.04) \times 10^{-10}$		
670.8		654.2	2.9	13.7		$(1.34 \pm 0.05) \times 10^{-10}$		
670.0		654.2	2.0	13.7		$(1.39 \pm 0.05) \times 10^{-10}$		
669.4		654.2	1.5	13.7		$(1.46 \pm 0.05) \times 10^{-10}$		
						k_1^{ave} (670Pa, He) = $(1.34 \pm 0.24) \times 10^{-10}$		
433.7	0.0	319.6	76.6	37.5			$(3.66 \pm 0.05) \times 10^{-11}$	
433.7	0.0	319.6	76.6	37.5			$(3.77 \pm 0.04) \times 10^{-11}$	
654.0	534.1	96.9	11.6	11.4			$(4.77 \pm 0.08) \times 10^{-11}$	
689.0	616.9	45.1	21.7	5.3			$(3.49 \pm 0.09) \times 10^{-11}$	
706.0	550.7	139.5	9.9	5.9			$(3.97 \pm 0.10) \times 10^{-11}$	
719.7	608.6	89.8	10.7	10.5			$(3.37 \pm 0.05) \times 10^{-11}$	
720.0	600.4	88.2	21.1	10.4			$(3.35 \pm 0.06) \times 10^{-11}$	
720.0	600.4	88.2	21.1	10.4			$(3.74 \pm 0.08) \times 10^{-11}$	
720.5	600.4	88.6	21.2	10.4			$(3.54 \pm 0.08) \times 10^{-11}$	
720.5	600.4	88.6	21.2	10.4			$(3.37 \pm 0.05) \times 10^{-11}$	
720.5	600.4	88.6	21.2	10.4			$(3.42 \pm 0.07) \times 10^{-11}$	
721.2	583.8	86.1	41.2	10.1			$(3.33 \pm 0.06) \times 10^{-11}$	
721.7	579.7	104.8	25.0	12.3			$(3.73 \pm 0.07) \times 10^{-11}$	
1344.2	1283.5	44.7	10.7	5.3			$(3.71 \pm 0.13) \times 10^{-11}$	
1346.5	1233.8	91.1	10.9	10.7			$(3.62 \pm 0.09) \times 10^{-11}$	
1346.5	1233.8	91.1	10.9	10.7			$(3.68 \pm 0.07) \times 10^{-11}$	
						k_3^{ave} [c] = $(3.7 \pm 1.0) \times 10^{-11}$		
705.7	530.0	134.1	9.6	5.6	26.4			$(3.93 \pm 0.06) \times 10^{-13}$
708.2	513.4	129.2	9.2	5.4	50.9			$(3.63 \pm 0.07) \times 10^{-13}$
705.6	492.7	125.0	8.9	5.3	73.7			$(3.49 \pm 0.04) \times 10^{-13}$
705.1	476.1	120.5	8.6	5.1	94.8			$(3.45 \pm 0.07) \times 10^{-13}$
705.1	476.1	120.5	8.6	5.1	94.8			$(3.46 \pm 0.04) \times 10^{-13}$
							k_7^{ave} (705 Pa, N_2)[d] = $(3.6 \pm 0.4) \times 10^{-13}$	

[a] Stated uncertainty of individual measurements is two standard deviations of the fit precision and does not propagate the uncertainty of absorption coefficients. [b] The weighted average rate coefficient is k_1^{ave}(1330 Pa, He) = $(1.75 \pm 0.06) \times 10^{-10}$ cm^3 $molecule^{-1}$ s^{-1}; however, because the data are limited, we report the larger uncertainty based on the uncertainty found for similar measurement sets. [c] Uncertainty is two standard deviations and propagates the uncertainty of $\sigma_{240}(C_3H_4Cl)$. [d] Uncertainty is two standard deviations and propagates the uncertainty of k_3 and $\sigma_{240}(C_3H_4ClO_2)$.

uncertainty of $\sigma_{240}(C_3H_4Cl)$. The model used to fit this decay data was comprised of reactions 1, 2, and 3. The pure second-order decay of the absorbance signal suggests a relatively simple kinetic model. Each signal trace was fit to find $[Cl]_0$, the photodissociation yield of Cl_2, and $k_3(C_3H_4Cl+C_3H_4Cl)$. According to the modeling results, the average photolysis event dissociated ~0.3% of the irradiated Cl_2. This photodissociation yield is in accord with the yield estimated from the measured photolysis flux and absorption cross section of Cl_2 at 351 nm.[16]

We conducted tests to observe contributions by secondary reactions involving allene and Cl_2. We recorded the signal decays using mixtures containing different concentrations of allene and Cl_2 (Table 1) and expanded our computational kinetic model to include the appropriate side reactions. The fits of these data provided no statistically meaningful coefficients for side reactions but did give consistent values for $k_3(C_3H_4Cl+C_3H_4Cl)$ and $[Cl]_0$. We conclude that the C_3H_4Cl radical is practically inert to allene. Because the kinetic model predicted that C_3H_4Cl formation under all conditions was essentially complete within 100 μs, Cl atom recombination ($k \approx 2 \times 10^{-15}$ cm^3 $molecule^{-1}$ s^{-1})[18] and conceivable reaction chains initiated by Cl atoms are effectively suppressed. The models did not include such processes.

Our data does not rule out the activity of a reaction between the C_3H_4Cl radical with molecular chlorine. At 298 K, the related reaction between allyl radical and Cl_2 is relatively slow ($k_{298} \approx 1.1 \times 10^{-14}$ cm^3 $molecule^{-1}$ s^{-1}) because it has an activation energy of 18 kJ mol^{-1}.[19,20] At 298 K, this reaction will conserve the C_3H_4Cl concentration though the reaction sequence:

$$C_3H_4Cl + Cl_2 \rightarrow C_3H_4Cl_2 + Cl \quad (6)$$

$$Cl + C_3H_4 (+M) \rightarrow C_3H_4Cl \quad (1b)$$

If active, we expect reaction 6 to produce 2,3-dichloro-1-propene. Under the experimental conditions of this study, the estimated pseudo-first-order rate of reaction **6** (based on the allyl

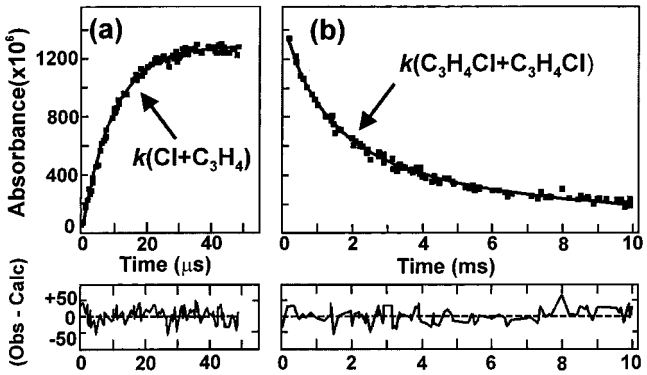

Figure 2. Plots of the transient absorbance at 240 nm observed when a mixture of Cl_2 and allene in N_2 buffer was photolyzed with 351 nm light at 298 K: (a) Squares in the upper trace show the increase of the C_3H_4Cl (2-chloroallyl) radical signal produced by the reaction, Cl + C_3H_4, at 655 Pa (4.9 Torr). The solid line in the upper trace shows the fit that gives one determination of the pseudo-first-order rate coefficient, $k(Cl+C_3H_4)$. The lower panel shows the plot of the residual differences between the observed signal and calculated signal obtained using the model. (b) Squares in the upper trace plot the pure second-order decay of C_3H_4Cl radical at 720 Pa (5.4 Torr) due to the recombination reaction 3. The solid line in the upper trace shows the fit of these data that provides one determination of the second-order rate coefficient, $k(C_3H_4Cl+C_3H_4Cl)$. The lower panel plots the residuals. Signal traces and residual traces are plotted on the same respective scales.

radical) was always 3 orders of magnitude smaller than that of reaction 1b; hence, we may conclude that the equilibrium concentration of atomic chlorine was insignificant and that the sequence of reactions 6 and 1b did not perturb the C_3H_4Cl concentration. Therefore, we did not include this catalytic reaction sequence in our models. We note that this reaction sequence may produce observable effects at higher temperatures, where the branching ratio of reaction 1 favors HCl formation.

Determination of $k(O_2 + C_3H_4Cl)$. The termolecular association of molecular oxygen with the 2-chloroallyl radical

$$C_3H_4Cl + O_2 (+M) \rightarrow C_3H_4ClO_2 \qquad (7)$$

was measured by adding various densities of excess O_2 to the flow mixture and monitoring optical absorbance at 240 nm. These experiments were conducted at a total pressure of 705 Pa in N_2 buffer and 298 K. Table 1 lists the experimental conditions and individual rate coefficients of these determinations.

Figure 3 shows two signal traces (squares) observed from mixtures containing different partial pressures of O_2. As a function of time, the absorbance decays are governed by the sum of second-order and first-order functions characterized by $k_3(C_3H_4Cl+C_3H_4Cl)$, $k_7(O_2+C_3H_4Cl)$, and $[O_2]$, the concentration of added O_2. Normally, we would expect the absorbance decay to converge on a zero baseline at long reaction times as the C_3H_4Cl concentration becomes depleted. However, cursory examination of Figure 3 shows that the signal trace decays to a nonzero baseline during the first 10 ms of reaction time. This behavior indicates that the $C_3H_4ClO_2$ product of reaction 7 carries significant absorption strength at 240 nm. This nonzero absorption displayed no apparent second-order decay, and the absorption signal finally disappeared at reaction times corresponding to the evacuation period of the flow reactor. Therefore, we conclude that the self-reaction rate of $C_3H_4ClO_2$ is extremely slow compared to the duration of a kinetic measurement. Because $C_3H_4ClO_2$ has no measurable reaction rate during each experiment, the concentration of $C_3H_4ClO_2$ at long reaction time is proportional to the amount of C_3H_4Cl consumed by reaction 7. After accounting for C_3H_4Cl consumed by reaction 3, the nonzero absorption baseline observed at long times in Figure 3 provides a direct measurement of $\sigma_{240}(C_3H_4ClO_2)$ relative to $\sigma_{240}(C_3H_4Cl)$.

To fit the decay data of each experiment, we used a kinetic model comprised of reactions 1, 2, 3, and 7 and maintained $k_3(C_3H_4Cl+C_3H_4Cl)$ and $k_1(Cl+C_3H_4)$ at their previously determined values (Table 1). Starting with a trial value of the absorption coefficient, $\sigma_{240}(C_3H_4ClO_2)$, each kinetic trace was fit to obtain a set of individual determinations of $[Cl]_0$ and $k_7(O_2+C_3H_4Cl)$. To determine the optimum $\sigma_{240}(C_3H_4ClO_2)$, we recursively adjusted $\sigma_{240}(C_3H_4ClO_2)$ and refit all of the individual experiments until we obtained the minimum of the residuals among all data and their simulations. This fitting procedure obtained $\sigma_{240}(C_3H_4ClO_2) = (3.6 \pm 0.7) \times 10^{-18}$ cm^2 and $k_7(O_2 + C_3H_4Cl) = (3.6 \pm 0.4) \times 10^{-13}$ cm^3 molecule^{-1} s^{-1} at 298 K and in 705 Pa (5.3 Torr) in N_2, where the uncertainties are two standard deviations and propagate the uncertainties of k_3 and $\sigma_{240}(C_3H_4Cl)$.

Computational Results

To construct the energy surface that governs the addition reaction of the chlorine atom to allene, we used the enthalpy of formation, $\Delta_f H^\circ_T$, of each relevant reactant, incipient radical, and secondary radical accessible through the reaction of the chlorine atom with allene (reaction 1). Table 2 lists the relevant $\Delta_f H^\circ_T$'s. Where possible, we report $\Delta_f H^\circ_T$(expt)'s, which are based on experimental data. We derived $\Delta_f H^\circ_T$(expt,allene) by combining the $\Delta_f H^\circ_T$(expt,propyne),[21] determined from the heat of combusion of propyne, with the experimentally determined heat of isomerization.[22,23] Many species have insufficient data for derivation of $\Delta_f H^\circ_T$(expt). For such species, we have used ab initio calculations to estimate $\Delta_f H^\circ_T$(calc).

The present calculations were performed with the Gaussian 94 program suite.[12] Initially, we used UHF//6-31G* calculations to find the stable structures. To find the minimum energy conformer of the 3-chloro-1-propene-2-yl radical isomer, we mapped the energy of its internal rotation by computing a UHF//6-31G* optimized structure every 15° along the internal rotation coordinate. These minimum energy structures were further refined with a series of G2 calculations as implemented by the Gaussian 94 program. These results yielded the G2 energy of each structure, H^{G2}, which was used to derive $\Delta_f H^\circ_T$(calc).

The $\Delta_f H^\circ_T$(calc)'s, listed in Table 2, were computed using the results of G2 calculations, and thus, were computed by assuming each species contains only harmonic oscillators and rigid rotors. To compensate for inaccuracies originating from spin contamination (which for all radicals did not exceed $S^2 = 0.759$ after projection of the highest spin contaminant, as compared to the ideal $S^2 = 0.75$) and correlation errors, we calculated $\Delta_f H^\circ_0$(calc) by combining the G2 energies, H_0^{G2}, and experimentally known heats of formation (Table 2) in reaction schemes. These standard methods for estimating $\Delta_f H^\circ_T$ are discussed elsewhere in greater detail.[24,25] We computed $\Delta_f H^\circ_0$(calc) for the 3-chloro-1-propene-2-yl radicals using isogyric reaction schemes based on reaction 1b. We computed $\Delta_f H^\circ_0$ for the chlorine substituted allyl radicals with isodesmic reactions involving the allyl radical, e.g.,

$$H_2C{=}CHCl + CH_2{\cdots}CH{\cdots}CH_2 \rightarrow H_2C{=}CH_2 + CH_2{\cdots}CCl{\cdots}CH_2 \qquad (12)$$

$$CH_3Cl + CH_2{\cdots}CH{\cdots}CH_2 \rightarrow CH_4 + CH_2{\cdots}CCl{\cdots}CH_2 \qquad (13)$$

TABLE 2: Experimental Data and G2 Computational Results Used to Estimate the Relative Energies of the Species Involved in the Cl + Allene System

species	H_0^{G2} hartree[a]	$H_{298.15}^{G2}$ hartree[a]	$\Delta_f H_0^\circ$(calc) kJ mol^{-1}	$\Delta_f H_{298.15}^\circ$(calc) kJ mol^{-1}	$\Delta_f H_0^\circ$(expt) kJ mol^{-1}	$\Delta_f H_{298.15}^\circ$(expt) kJ mol^{-1}
(*E*)-1-chloroallyl radical (C_s)	−576.159708	−576.153792	147.3 ± 3.4	138.1 ± 3.4		
(*Z*)-1-chloroallyl radical (C_s)	−576.160498	−576.15476	145.2 ± 3.4	135.6 ± 3.4		
(*E*)-1-chloro-1-propene-2-yl radical (C_s)	−576.122594	−576.11632	245.7 ± 1.1	237.5 ± 1.1		
(*Z*)-1-chloro-1-propene-2-yl radical (C_s)	−576.125613	−576.119428	237.8 ± 1.1	229.3 ± 1.1		
2-chloroallyl cation (C_{2v})	−575.851014	−575.845498	(962 ± 4)[b]			
2-chloroallyl radical (C_{2v})	−576.1591375	−576.153422	148.8 ± 3.4	139.1 ± 3.4		
3-chloro-1-propene-2-yl radical (C_s)	−576.122092	−576.116126	246.5 ± 2.3	237.5 ± 2.3		
allyl cation (C_{2v})	−116.708706	−116.703913			[966 ± 4][c]	
allyl radical (C_{2v})	−117.005896	−117.000936			(182 ± 3)[d]	(171 ± 3)[e]
allene (D_{2d})	−116.417840	−116.413085			(195.9 ± 2.3)[d]	(188.3 ± 2.3)[f]
methyl chloride (C_{3v})	−499.553828				(−73.94 ± 0.6)[g]	
propyne (C_{3v})	−116.41917[h]				(192.5 ± 0.9)[i]	(184.5 ± 0.9)[i]
vinyl chloride (C_s)	−537.568284				(30.57 ± 2.1)[g]	(23.0 ± 2.1)[g]
Cl	−459.6779656[j]	−459.6756052[j]			(119.621 ± 0.006)[k]	(121.301 ± 0.008)[k]

[a] 1 hartree = 2625.53 kJ mol^{-1}. [b] On the basis of $IE_a(C_3H_4Cl) = 8.43 \pm 0.02$ eV derived using H_0^{G2}'s and adjusted using $IE_a(C_3H_5) = 8.13 \pm 0.02$ eV from ref 27; see text. [c] Derived using $\Delta_f H_0^\circ$(expt, allyl), H_0^{G2}'s, and $IE_a(C_3H_5) = 8.13 \pm 0.02$ eV from ref 27 and standard states of ref 41. [d] Computed using the estimated $\Delta_f H_{298.15}^\circ$(expt), the heat function derived from $H_0^{G2} - H_{298.15}^{G2}$, and standard states of ref 41. [d] From ref 26. [f] Computed using $\Delta_f H_{298.15}^\circ$(expt, propyne) and the enthalpy of isomerization that was reported in ref 22 and reanalyzed in ref 23. [g] From ref 42. [h] From ref 43. [i] From ref 21 [j] A correction of $E = -0.013382$ hartree is added to account for the spin−orbit energy. [k] From ref 41.

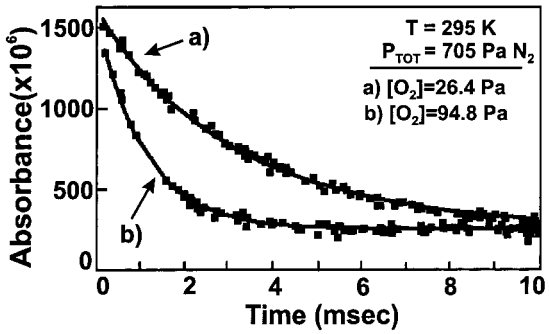

Figure 3. Plots of the transient absorbance observed at 240 nm following the 351 nm photolysis of mixtures of Cl_2, N_2, allene, and O_2. (a) Trace of the decay with 26.4 Pa of added O_2. (b) Trace of the decay with 94.8 Pa of added O_2. For both plots the total pressure is 705 Pa (5.3 Torr) of N_2 and the partial pressures of Cl_2 and allene are nominally the same (Table 1).

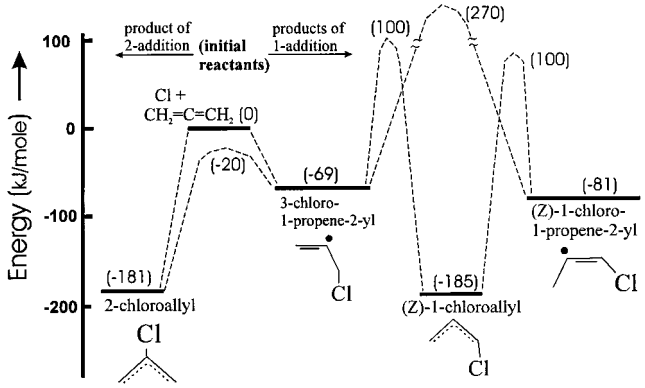

Figure 4. Energy diagram of the reactants and radical products that are energetically accessible from the addition reaction, Cl + allene. Dashed lines indicate the isomerization paths associated with the transfer of a hydrogen atom or a chlorine atom between two carbon atoms. Each stable radical structure and isomerization transition state is annotated with its energy (in kJ mol^{-1}) relative to the reactants (Cl + CH_2=C=CH_2) at 0 K. The isomerization energy barriers are from ref 7. See text and Table 2.

These computations used $\Delta_f H_0^\circ$(allyl), which we calculated using $\Delta_f H_{298.15}^\circ$(allyl) = 171 ± 3 kJ mol^{-1}, recently recommended by Tsang[26] from an evaluation of extensive experimental data.

Table 2 lists the G2 energies of the allyl cation and 2-chloroallyl cation ground state ($\tilde{X}^2A_1$) structures. The G2 energies predict that the first adiabatic ionization energy from the $\tilde{X}^2A_2$ state of allyl radical is $IE_a^{G2}(C_3H_5) = 8.09$ eV. For comparison, photoelectron experiments obtained $IE_a(C_3H_5) = 8.13 \pm 0.02$ eV. [27] For the 2-chloroallyl ($\tilde{X}^2A_2$) radical, the G2 energies predict $IE_a^{G2}(C_3H_4Cl) = 8.38$ eV. Using the correction implied by the allyl radical results, we predict $IE_a(C_3H_4Cl) = 8.43 \pm 0.02$ eV. Table 2 lists $\Delta_f H_T^\circ$'s computed using the experimental IE_a of the allyl cation and the estimated IE_a of the 2-chloroallyl cation.

Discussion

The CRD spectrum observed between 252 nm and our instrument limit of 238 nm (Figure 1) is assigned to the 2-chloroallyl radical for which no spectroscopic data are currently available. The present data are only sufficient to support simple concentration measurements. The observation of an absorption spectrum of the 2-chloroallyl radical is not surprising because the analogous allyl radical also exhibits a complicated spectrum over this energy interval originating from several, strongly coupled, electronic states.[28−31] The nonradiative and dissociative processes of these states are under active investigation by other groups.[32−34] Since the higher electronic states of allyl radical contain Rydberg character[35] and such states tend to shift with ionization energy, the slightly higher IE_a of the 2-chloroallyl radical suggests that its absorption envelope is blue shifted relative to that observed in the allyl radical.

Reactive Pathways Available to Cl + Allene. Figure 4 diagrams the relative energies of the reactants and energetically accessible products via the addition reaction of Cl and allene (reaction 1). Figure 4 also shows the structure of each transient species. This diagram was constructed using the experimentally and computationally derived values of $\Delta_f H_0^\circ$ listed in Table 2. The energy of each product channel (at 0 K), relative to the reactants, is shown in parentheses. Figure 4 shows only the energies and structures of the most stable radical isomers. The differences of $\Delta_f H_0^\circ$(calc)'s among analogous isomers range between 1 and 8 kJ mol^{-1} (Table 2) and are too small to change the outcome of reaction 1.

Dashed lines in Figure 4 symbolize the isomerization paths and energy barriers associated with a shift of a hydrogen or a chlorine atom among the carbons. Each isomerization energy

barrier was computed from the average of the energy differences between each relevant, optimized, stationary transition state structure and the initial and final radical structures. These energies were computed with a QCISD(T)/6-311+G**//QCISD/6-31+G** procedure and the calculations include appropriate zero-point vibrational energy contributions obtained by MP2/6-31+G** calculations. The computational research that determined these transition structures is reported elsewhere.[7]

Calculations of the transition state structures indicate that negligible energy barriers impede chlorine atom addition at the center and end carbons. [7] Chlorine addition to an end carbon forms the 3-chloro-1-propene-2-yl radical. Addition onto the center carbon forms the 2-chloroallyl radical directly. Therefore, we restate reaction 1 more accurately as

$$H_2C{=}C{=}CH_2 + Cl\ (+M) \rightarrow HCl + C_3H_3 \quad (1a)$$

$$\rightarrow CH_2Cl{-}\dot{C}{=}CH_2 \quad (1b_1)$$

$$\rightarrow CH_2{\cdots}CCl{\cdots}CH_2 \quad (1b_2)$$

where the subscript designation denotes the carbon atom involved in the chlorine addition. Since reactions $1b_1$ and $1b_2$ are governed by different potential energy surfaces, the nascent abundance of 3-chloro-1-propene-2-yl and 2-chloroallyl radicals is not predictable without explicit dynamics calculations. Nevertheless, since addition at the end and center carbons is unhindered by energy barriers, we expect the nascent ensemble of reaction 1b products to contain abundant fractions of both radicals.

Since all members of the incipient ensemble are chemically activated, each product radical contains an internal energy greater than or equal to its formation enthalpy. For initial reactants at 298 K, all 3-chloro-1-propene-2-yl radicals contain ~69 kJ mol^{-1} and all 2-chloroallyl radicals contain ~181 kJ mol^{-1}. Figure 4 accounts for the available internal energy of all isomers by referencing all isomer structures and isomerization paths to the energy of the initial reactants, i.e., Cl + allene are at 0 kJ mol^{-1}. Reaction paths that remain below the reference energy (0 kJ mol^{-1}) are energetically accessible to the entire incipient C_3H_4Cl ensemble. Those reaction paths crossing into positive energy are inaccessible to most of the incipient C_3H_4-Cl ensemble.

Unimolecular processes in the C_3H_4Cl complex lead to other isomers. By shifting a hydrogen atom, the incipient 3-chloro-1-propene-2-yl radical may isomerize forming 1-chloroallyl and 1-chloro-1-propene-2-yl radicals. However, substantial isomerization barriers of energies greater than 100 kJ mol^{-1} impede these isomerization paths.[7] We conclude that isomerization through hydrogen transfer is unimportant at ambient temperature.

The adduct radicals isomerize by transferring the chlorine atom, i.e.,

$$C^{\alpha}H_2{-}\dot{C}^{\beta}{=}C^{\gamma}H_2{-}Cl \rightleftarrows C^{\alpha}H_2{\cdots}C^{\beta}Cl{\cdots}C^{\gamma}H_2 \quad (14)$$

As diagramed in Figure 4, isomerization between 3-chloro-1-propene-2-yl ($C^{\alpha}H_2{=}C^{\beta}{-}C^{\gamma}H_2{-}Cl$) and 2-chloroallyl radicals occurs at an energy that is lower than the initial reactants. Computational evidence indicates that the isomerization between vinyl and allyl structures does not proceed through a transition state described by a saddle point. Instead, as a function of $\angle(C^{\beta}{-}C^{\gamma}{-}Cl)$ angle, the potential energies of the 3-chloro-1-propene-2-yl and 2-chloroallyl ground-state radicals increase and intersect near $\angle(C^{\beta}{-}C^{\gamma}{-}Cl) = 58.5°$. These surfaces are coupled through the torsion of the $C^{\gamma}H_2$ group. For example, near $\angle(C^{\beta}{-}C^{\gamma}{-}Cl) = 58.5°$ the plane of the $C^{\gamma}H_2$ group within the 3-chloro-1-propene-2-yl radical is approximately perpendicular to the plane containing the carbon and chlorine atoms. The 3-chloro-1-propene-2-yl and 2-chloroallyl isomers remain distinct, but rotation of the $C^{\gamma}H_2$ group by ~90° places the Cl atom onto the potential energy surface corresponding to direct attack at the center carbon, thus forming 2-chloroallyl radical. We discovered evidence for the surface intersection with transition state calculations at the QCISD/6-31+G** level which found a second order saddle point. Attempts to locate a saddle point by following the imaginary roots lead discontinuously to each isomer. When the dihedral coordinate of the $C^{\gamma}H_2$ group was frozen, two series of relaxed energy scan calculations over a set of $\angle(C^{\beta}{-}C^{\gamma}{-}Cl)$ angles, corresponding to forward and reverse isomerization between the 3-chloro-1-propene-2-yl and 2-chloroallyl isomers, found distinct adiabatic potentials. When the dihedral coordinate of the $C^{\gamma}H_2$ torsion was also allowed to relax, the adiabatic potentials coupled through discontinuous $C^{\gamma}H_2$ rotation and the resultant isomerization paths proceeded at energies below the initial reactants, Cl + allene.

We estimate that the surface intersections lie about 20 kJ mol^{-1} lower in energy than the initial reactants (Figure 4).[7] This estimate is based upon QCISD/6-31+G** calculations of the second-order saddle point for isomerization and upon the minimum energy observed for discontinuous $C^{\gamma}H_2$ rotation. Details of this study are reported elsewhere.[7] Because all chemically activated, incipient radicals contain sufficient internal energy to promote the isomerization (reaction 14), equilibrium exists between the C_3H_4Cl isomers. Since the 2-chloroallyl radical is ~112 kJ mol^{-1} more stable than the 3-chloro-1-propene-2-yl radical, the equilibrium ensemble is composed almost completely of 2-chloroallyl radical. Consequently, we conclude that regardless of the site of chlorine addition, the dominant product of reaction 1b is the 2-chloroallyl radical.

Interpretation of the Rate Coefficients. The 298 K rate coefficients of reaction 1 (Table 1) obtained here are consistent with the earlier measurements[3,36] and indicate that chlorine atoms add to allene at nearly the gas-kinetic limit. The results of ab initio calculations are in accord with these results since they have predicted that chlorine atoms encounter negligibly small barriers as they add to allene.[7] It should be noted that although the production of HCl (the channel observed by Farrell and Taatjes[3]) is minimal at ambient temperatures, the overall Cl atom addition rate coefficient determined by their method would be expected to be comparable to our results for similar pressures of the same buffer gas. Each low-pressure bimolecular rate coefficient determination should be viewed as an independent result for a given third-body stabilization efficiency (i.e., degree of pressure falloff.) As expected, the bimolecular rate coefficient increases with increasing pressure of He buffer (Table 1) and is greater at a given pressure in nitrogen buffer than in helium. Also, the value obtained by Farrell,[3] $k_1 = (2.49 \pm 0.52) \times 10^{-10}$ cm^3 molecule^{-1} s^{-1} in approximately 1333 Pa of CO_2 is significantly larger than our highest pressure helium result. The rate coefficient obtained by Wallington[36] $k_1 = (4.38 \pm 0.26) \times 10^{-10}$ cm^3 molecule^{-1} s^{-1} at near atmospheric pressure of nitrogen should be regarded as a close approximation to the high-pressure limit. More study of the pressure dependence of the reaction rate coefficient would be necessary to refine the low- and high-pressure limits.

For the self-reaction of the chlorine atom adduct (reaction 3), we obtain a pressure-independent rate coefficient of $(3.7 \pm 1.0) \times 10^{-11}$ cm^3 molecule^{-1} s^{-1} at 298 K. Because the ab initio results indicate that the only persistent chlorine addition product of reaction 1 is the 2-chloroallyl radical, we assign the observed self-reaction rate coefficient, $k_3(C_3H_4Cl+C_3H_4Cl)$, as a fundamental rate coefficient of 2-chloroallyl radical. We believe that the present determinations of $k_3(C_3H_4Cl+C_3H_4Cl)$ and $k_7(O_2+C_3H_4Cl)$ are the first rate coefficients reported for this

radical. The measurement of k_3 may be compared to rate coefficients of other allyl radicals. The recommended self-reaction rate coefficient of the allyl radical[37] is 2.65×10^{-11} cm^3 molecule^{-1} s^{-1}. A recent result from our laboratory indicates that the self-reaction rate coefficient for the 1,2-dichloroallyl ($C_3H_3Cl_2$) radical, formed by addition of a Cl atom to propargyl chloride, is $(3.4 \pm 0.9) \times 10^{-11}$ cm^3 molecule^{-1} s^{-1}.[38] Because the gas kinetic collision rate diminishes with increasing chlorination, the larger rate coefficients of the chloroallyl radicals are surprising and indicate that chlorine substitution increases the inherent reactivity of the substituted allyl radicals.

The reaction rate coefficient for the oxygen addition to the 2-chloroallyl radical measured here is notable in that its magnitude is comparable to, or slightly less than, that measured for the allyl radical. The only room-temperature rate coefficient measurement of which we are aware for oxygen addition to allyl radical obtained $(6 \pm 2) \times 10^{-13}$ cm^3 molecule^{-1} s^{-1} at approximately ambient pressure of synthetic air ($N_2 + O_2$).[39] The difference between this result and our reported result of $k_7 = (3.6 \pm 0.4) \times 10^{-13}$ cm^3 molecule^{-1} s^{-1} can be attributed either to the difference in the total pressure or to the inherent differences in reactivity between the 2-chloroallyl radical and the allyl radical, or perhaps, some combination of the two. The magnitude of $\sigma_{240}(C_3H_4ClO_2)$ and the relative low reactivity of the $C_3H_4ClO_2$ radical with itself are both as expected, based on the available knowledge concerning peroxy radicals.[40] Presumably, the rate coefficient for oxygen addition to the 2-chloroallyl radical would be greater than that to allyl at a given pressure due to the decreased resonance stabilization, which can greatly affect these rates. Clearly, more study of the effects of chlorine substitution on the reactivity of these small unsaturated hydrocarbon radicals is needed to fully characterize these interesting chemical systems.

Conclusion

Experiments and ab initio calculations have characterized the mechanism and rate coefficients for chlorine atom addition to allene. The observed rate coefficients show that a chlorine atom adds rapidly to allene at 298 K. Ab initio results indicate that chlorine addition may occur at the terminal and center unsaturated carbon atoms forming the 3-chloro-1-propene-2-yl and 2-chloroallyl radicals. Initially, these radicals contain sufficient internal energy to establish equilibrium. Since this equilibrium greatly favors the 2-chloroallyl radical, the dominant reaction product is the 2-chloroallyl radical. The 2-chloroallyl radical exhibits a continuum absorption that has an onset at 252 nm and extends to wavelengths shorter than 238 nm. By using cavity ring-down spectroscopy, we have measured the absorption cross section of the 2-chloroallyl radical and determined rate coefficients for its formation by Cl + allene, for its recombination reaction, and for its reaction with O_2.

Acknowledgment. We thank Dr. Russell D. Johnson III and Dr. Carlos Gonzales for assistance and advice with the ab initio calculations. We thank Dr. Wing Tsang and Dr. Jeffrey Manion for insightful discussions.

References and Notes

(1) Tsang, W. *Combust. Sci. Technol.* **1990**, *74*, 99.

(2) Wallington, T. J.; Skewes, L. M.; Siegl, W. O. *J. Photochem. Photobiol. A: Chem.* **1988**, *45*, 167.

(3) Farrell, J. T.; Taatjes, C. A. *J. Phys. Chem. A* **1998**, *102*, 4846.

(4) Atkinson, D. B.; Hudgens, J. W. *J. Phys. Chem. A* **1999**, *103*, 4242.

(5) Griesbaum, K.; Oswald, A. A.; Hall, D. N. *J. Org. Chem.* **1964**, *29*, 2404.

(6) Kovachic, D.; Leitch, L. C. *Can. J. Chem.* **1961**, *39*, 363.

(7) Hudgens, J. W.; Gonzalez, C. Chlorination Chemistry. 3. Ab initio Study of the Potential Energy Surface Governing the Reaction of Chlorine and Allene and Isomerization within the C_3H_4Cl Unsaturated Radical. In preparation.

(8) Certain commercial materials and equipment are identified in this paper in order to adequately specify the experimental procedure. Such identification neither implies recommendation or endorsement by the National Institute of Standards and Technology nor does it imply that the material or equipment identified is the best available for the purpose.

(9) Atkinson, D. B.; Hudgens, J. W. *J. Phys. Chem. A* **1997**, *101*, 3901.

(10) Braun, W. *Int. J. Chem. Kinet.* **1988**, *20*, 51.

(11) *Nonlinear Levenberg−Marquardt fitting virtual instrument*, Labview 4.0; National Instruments Corporation: Austin, TX, 1994−1995.

(12) Frisch, M. J.; Trucks, G. W.; Schlegel, H. B.; Gill, P. M. W.; Johnson, B. G.; Robb, M. A.; Cheeseman, J. R.; Keith, T.; Petersson, G. A.; Montgomery, J. A.; Raghavachari, K.; Al-Laham, M. A.; Zakrzewski, V. G.; Ortiz, J. V.; Foresman, J. B.; Cioslowski, J.; Stefanov, B. B.; Nanayakkara, A.; Challacombe, M.; Peng, C. Y.; Ayala, P. Y.; Chen, W.; Wong, M. W.; Andres, J. L.; Replogle, E. S.; Gomperts, R.; Martin, R. L.; Fox, D. J.; Binkley, J. S.; Defrees, D. J.; Baker, J.; Stewart, J. P.; Head-Gordon, M.; Gonzalez, C.; Pople, J. A. *Gaussian 94*, revision D.4; Gaussian, Inc.: Pittsburgh, PA, 1995.

(13) Ramsay, D. A.; Thistlethwaite, P. *Can. J. Phys.* **1966**, *44*, 1381.

(14) Jacox, M. E.; Milligan, D. E. *Chem. Phys.* **1974**, *4*, 45.

(15) Hodges, J. T.; Looney, J. P.; van Zee, R. D. *Appl. Opt.* **1996**, *35*, 4112.

(16) DeMore, W. B.; Sander, S. P.; Golden, D. M.; Hampson, R. F.; Kurylo, M. J.; Howard, C. J.; Ravishankara, A. R.; Kolb, C. E.; Molina, M. J. *Chemical Kinetics and Photochemical Data for Use in Stratospheric Modeling*; NASA, 1994.

(17) Lightfoot, P. D.; Cox, R. A.; Crowley, J. N.; Destriau, M.; Hayman, G. D.; Jenkin, M. E.; Moortgat, G. K.; Zable, F. *Atmos. Environ.* **1992**, *26A*, 1085.

(18) Baulch, D. L.; Duxbury, J.; Grant, S. J.; Montague, D. C. *J. Phys. Chem. Ref. Data* **1981**, *10* (Suppl)

(19) Timonen, R. S.; Russell, J. J.; Sarzynski, D.; Gutman, D. *J. Phys. Chem.* **1987**, *91*, 1873.

(20) Timonen, R. *Ann. Acad. Sci. Fenn. Ser. A2* **1988**, *218*, 5.

(21) Wagman, D. D.; Kilpatrick, J. E.; Pitzer, K. S.; Rossini, F. D. *J. Res. NBS* **1945**, *35*, 467.

(22) Cordes, J. F.; Gunzler, H. *Chem. Ber.* **1959**, *92*, 1055.

(23) Cox, J. D.; Pilcher, G. *Thermochemistry of Organic and Organometallic Compounds*; Academic Press: New York, 1970.

(24) Johnson, R. D., III; Hudgens, J. W. *J. Phys. Chem.* **1996**, *100*, 19874.

(25) *Computational Thermochemisty: prediction and estimation of molecular thermodynamics*; Irikura, K. K., Frurip, D. J., Eds.; American Chemical Society: Washington, DC, 1998; Vol. 677.

(26) Tsang, W. Heats of Formation of Organic Free Radicals by Kinetic Methods in Energetics of Organic Free Radicals. In *Energetics of Organic Free Radicals*; Simoes, J. A., Greenberg, A., Liebman, J. F., Eds.; Blackie Academic and Professional: London, 1996; pp 22−58.

(27) Houle, F. A.; Beauchamp, J. L. *J. Am. Chem. Soc.* **1978**, *100*, 3290.

(28) Hudgens, J. W.; Dulcey, C. S. *J. Phys. Chem.* **1985**, *89*, 1505.

(29) Sappey, A. D.; Weisshaar, J. C. *J. Phys. Chem.* **1987**, *91*, 3731.

(30) Blush, J. A.; Minsek, D. W.; Chen, P. *J. Phys. Chem.* **1992**, *96*, 10150.

(31) Getty, J. D.; Liu, X.; Kelly, P. B. *J. Phys. Chem.* **1992**, *96*, 10155.

(32) Deyerl, H.-J.; Gilbert, T.; Fischer, I.; Chen, P. *J. Chem. Phys.* **1997**, *107*, 3329.

(33) Deyerl, H.-J.; Fischer, I.; Chen, P. *J. Chem. Phys.* **1999**, *110*, 1450.

(34) Stranges, D.; Stemmler, M.; Yang, X.; Chesko, J. D.; Suits, A. G.; Lee, Y. T. *J. Chem. Phys.* **1998**, *109*, 5372.

(35) Ha, T. K.; Oth, J. F. M. *J. Phys. Chem.* **1986**, *85*, 1439.

(36) Wallington, T. J.; Andino, J. M.; Lorkovic, I. M.; Kaiser, E. W.; Marston, G. *J. Phys. Chem.* **1990**, *94*, 3644.

(37) Tsang, W. *J. Phys. Chem. Ref. Data* **1991**, *20*, 221.

(38) Atkinson, D. B.; Hudgens, J. W. **1999**, *J. Phys. Chem.* **1999**, *103*, 7978.

(39) Jenkin, M. E.; Murrells, T. P.; Shalliker, S. J.; Hayman, G. D. *J. Chem. Soc., Faraday Trans.* **1993**, *89*, 433.

(40) Wallington, T. J.; Dagaut, P.; Kurylo, M. J. *J. Photochem. Photobiol. A: Chem.* **1988**, *42*, 173.

(41) Chase, M. W., Jr.; Davies, C. A.; Downey, J. R., Jr.; Frurip, D. J.; McDonald, R. A.; Syverud, A. N. *J. Phys. Chem. Ref. Data* **1985**, *14*.

(42) Gurvich, L. V.; Veyts, I. V.; Alcock, C. B. *Thermodynamic Properties of Individual Substances*, 4th ed.; Hemisphere Publishing Corp.: New York, 1991; Vol. 2.

(43) Curtiss, L. A.; Raghavachari, K.; Redfern, P. C.; Pople, J. A. *J. Chem. Phys.* **1997**, *106*, 1063.